Novel $\mathrm{TE}_{10\delta}$ Rectangular-Waveguide-Type Resonators and Their Bandpass Filter Applications

Hee Yong Hwang, *Member, IEEE,* and Sang-Won Yun, *Member, IEEE*

***Abstract*—New dielectric-filled rectangular-waveguide-type $\mathrm{TE}_{10\delta}$ resonators are presented. A dielectric-filled rectangular waveguide section (WGS) has inductive impedance at the open-end faces. Using this property and the frequency dependency of the wave impedance of the WGS, we calculated the resonant frequency and the slope parameter of the waveguide-type resonators. The resonant frequency depends strongly on the width of the WGS and loosely on the height and the length. The calculated resonant frequencies agree well with measured data. One of the proposed bandpass filters shows highly reduced spurious up to three times the center frequency. Quality factors of the resonator and effects of a housing are also discussed.**

***Index Terms*—BPF, dielectric resonator, $\mathrm{TE}_{10\delta}$, waveguide filter, waveguide resonator.**

I. Introduction

DIELECTRIC materials with a high dielectric constant, high Q, as well as low temperature coefficient have been developed and widely adopted for many types of miniaturized resonators. Using these materials, we can easily form small high-Q dielectric-filled waveguide resonators. Such resonators are typically based on the resonance characteristics around either quarter wavelength or half wavelength [1]–[6].

However, when a dielectric-filled waveguide section (WGS) is terminated by proper impedance at both ends, we can find impedance-matched points or resonant frequencies, depending on the terminated impedance conditions. This resonance can be observed in dielectric-filled WGS of very small electrical length and can be called as $\mathrm{TE}_{10\delta}$ mode because of its short physical and electrical length. Due to the leakage of the electromagnetic field from the open-end face (OEF), the perfect magnetic wall (PMW) is shifted from the OEF into the interior of the resonator [5]. Each OEF can be read as an inductive load, which can also make a very short WGS work as a resonator. The investigation of the OEF characteristics and an equivalent resonator model is needed to obtain resonator parameters such as the resonant frequency and the slope parameter. The radiation from the OEFs and the effect of a housing have to be also considered for the practical use of the resonators. The resonator could be also designed as a planar surface-mount device (SMD) because the resonant frequency is hardly changed by a variation of the height "b" of the WGS.

Manuscript received September 1, 2000. This work was supported by KOSEF under the European Research Council Program through the MINT Research Center at Dongguk University.

H. Y. Hwang is with the Department of Electronic Engineering, University of Maryland at College Park, College Park, MD 20742 USA (e-mail: heyhwang@hotmail.com).

S.-W. Yun is with the Department of Electronics Engineering, Sogang University, Seoul, Korea.

Publisher Item Identifier 10.1109/TMTT.2002.800445.

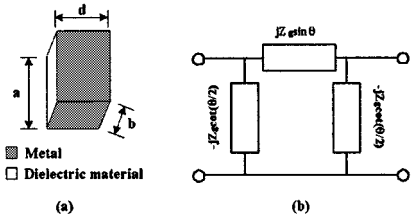

Fig. 1. (a) WGS with dimensions $a \times b \times d$ and (b) its equivalent circuit. The OEFs are considered as PMWs.

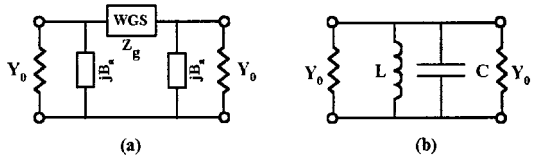

Fig. 2. (a) WGS and (b) lumped *LC* resonator with load Y_0.

II. WGS With OEFs

A. Resonant Modes of a Dielectric-Filled Rectangular WGS

A structure of dielectric-filled rectangular WGS and its equivalent circuit are shown in Fig. 1(a) and (b), respectively. The OEFs of the WGS are considered as PMWs in the figure. Considering the leakages [5] of the electromagnetic field from both OEFs of the rectangular WGS as two additional susceptance B_a's, more practically, we can derive a lumped *LC* resonator model of the WGS with arbitrary loads Y_0, as shown in Fig. 2.

Using the equivalent circuit of WGS in Fig. 1 we can derive the S-parameters of WGS and *LC* resonator with load Y_0, respectively, as follows:

$$|S_{21}|^2_{\mathrm{WG}} = \frac{1}{1+\left(\frac{1}{2Y_0}\right)^2\left[2B_a\cos\theta+\left(Y_g-\frac{Y_0^2}{Y_g}-\frac{B_a^2}{Y_g}\right)\sin\theta\right]^2} \tag{1}$$

$$|S_{21}|^2_{\mathrm{LC}} = \frac{1}{1+\left(\frac{B}{2Y_0}\right)^2}$$
$$B = j\left(\omega C-\frac{1}{\omega L}\right) \tag{2}$$

where $|S21|_{\mathrm{WG}}$ and $|S21|_{\mathrm{LC}}$ represent the amplitudes of S_{21}s of the Fig. 2(a) and (b), respectively, when the loads are Y_0.

Compared the two equations with each other, the equivalent susceptance B is derived as

$$B = Y_0 \left[\frac{2B_a \cos\theta}{Y_0} - \left(\frac{Y_0}{Y_g} - \frac{Y_g}{Y_0} + \frac{B_a^2}{Y_0 Y_g} \right) \sin\theta \right]. \quad (3)$$

If we set the resonant condition to be $B = 0$, then the electrical length of the waveguide resonator at the resonant frequency is given by (4). Using a root-finding algorithm, the resonant frequency f_0 is from (3) as shown in (5)

$$\theta_0 = \tan^{-1} \frac{2B_a Y_g}{Y_0^2 - Y_g^2 + B_a^2} \quad (4)$$

$$f_0 = f|_{B=0} \quad (5)$$

where Y_g is the characteristic admittance of the WGS

The susceptance slope parameter $\overline{b}$ is defined as (6)

$$\overline{b} = \frac{f_0}{2} \left. \frac{\partial B}{\partial f} \right|_{f=f_0} \approx \frac{f_0}{2} \left. \frac{\Delta B}{\Delta f} \right|_{f=f_0}. \quad (6)$$

In the above equations, the resonant frequency and the susceptance B are dependent on the electrical length θ, the characteristic admittance of the WGS Y_g, additional susceptance B_a and the load Y_o.

When B_a is zero, as the approach to resonators with PMWs at both ends, then (3) is simplified as (7)

$$B = Y_0 \left[\left(\frac{Y_g}{Y_0} - \frac{Y_0}{Y_g} \right) \sin\theta \right]. \quad (7)$$

Equation (7) expresses the susceptance of an ideal waveguide resonator when real loads are attached at its open ends, and it has two solutions for resonance condition, $B = 0$.

First, as a conventional resonator, if zero value is chosen for Y_0 when OEF is under open or PMW condition it can be more compact equation as Cohn [7] described for the rectangular waveguide TE_{101} resonant mode

$$B = Y_g \sin\theta. \quad (8)$$

At the resonant frequency, the electrical length θ, the resonant frequency ω_0, and the susceptance slope parameter $\overline{b}$ can be expressed as in (9) and (10), the well-known equations for TE_{mnk} resonant modes

$$\theta = k\pi, \qquad k = 1, 2, 3, \cdots \quad (9)$$

$$\omega_0 = \frac{1}{\sqrt{\mu\varepsilon}} \sqrt{\left(\frac{m\pi}{a}\right)^2 + \left(\frac{n\pi}{b}\right)^2 + \left(\frac{k\pi}{d}\right)^2}, \quad k = 1, 2, 3, \cdots \quad (10)$$

$$\overline{b} = \frac{\omega_0}{2} \left. \frac{dB}{d\omega} \right|_{\omega_0} = \frac{\pi\omega_0\varepsilon}{2\beta d_z} \text{ or } \frac{\pi Y_g}{2} \left(\frac{\lambda_{g0}}{\lambda_0} \right)^2 \quad (11)$$

where $Z_g = (\omega\mu/\beta)\, d_z$, $d_z = d_r(b/a)$, d_r is a constant, and, λ_0 and λ_{g0} are the wavelengths in free space and in empty waveguide, respectively. It is difficult to define waveguide characteristic impedance Z_g uniquely. There are at least three different ways to define the impedance, and one of the definitions must be used consistently [8]–[10]. When the "power-voltage" definition is used, the parameter d_r will be 2. If the wave impedance is chosen for calculation, then d_r is a/b. In this paper, the "power-voltage" definition is used consistently.

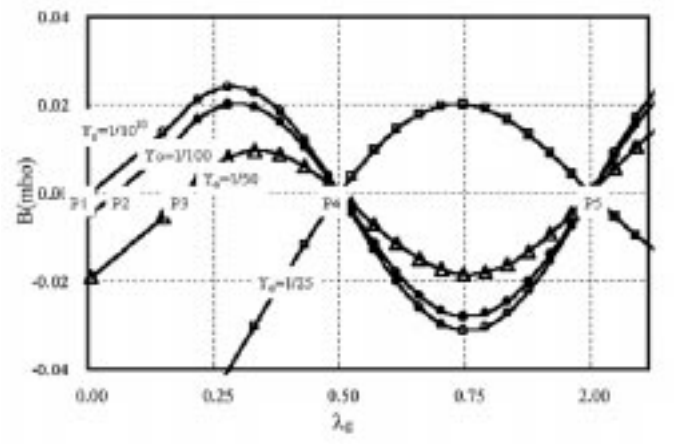

Fig. 3. Susceptance B versus wavelength λ_g; $\varepsilon_r = 38.4$, $a \times b \times d = 20 \times 5 \times 10$ (mm), $B_a = 0$, and $f_c = 1.210$ GHz.

When we consider a distributed resonator, the effect of load Y_0 is frequently neglected for simplicity, as in the case of an ideal LC resonator, and the value is treated as zero. However, the load can change the characteristics of the resonator, such as resonant frequency, slope parameter and quality factor, occasionally. To obtain a more exact solution, we should use $Y_0 \neq 0$ condition. Supposed that Y_g is not to be equal to Y_0, the resultant susceptance slope parameter $\overline{b}$ can be written as

$$\overline{b} = \frac{f_0}{2} \left. \frac{\partial B}{\partial f} \right|_{f_0} = \frac{Y_0}{Y_g} \left(\frac{Y_0}{Y_g} - \frac{Y_g}{Y_0} \right) \frac{\pi\omega_0\varepsilon}{2\beta d_z} \text{ or } \frac{\pi Y_0}{2} \left(\frac{Y_0}{Y_g} - \frac{Y_g}{Y_0} \right) \left(\frac{\lambda_{g0}}{\lambda_0} \right)^2. \quad (12)$$

Second, (7) has another solution when waveguide characteristic impedance is equal to the load impedance

$$Y_g = Y_0 \quad (13)$$

$$\omega_0 = \frac{K_c}{\sqrt{\mu\varepsilon - (\mu Y_0 d_z)^2}}. \quad (14)$$

where $K_c = \sqrt{(m\pi/a)^2 + (n\pi/b)^2}$.

The corresponding susceptance slope parameter $\overline{b}$ is

$$\overline{b} = \frac{\omega_0}{2} \left. \frac{dB}{d\omega} \right|_{\omega_0} = \frac{\omega_0\varepsilon}{\beta d_z} \left(\frac{K_c}{K} \right)^2 \sin\theta. \quad (15)$$

We can read (14) as an equation for "impedance matching frequency." This concept could be true with any waveguide that the characteristic impedance is changed by frequency, differently from TEM mode lines.

Using (3) with $B_a = 0$ or (7), the susceptance B is plotted in Fig. 3, according to some Y_0 values. The zero crossing points, P4 ($\lambda_g = 0.5$) and P5 ($\lambda_g = 1.0$) in the figure, represent TE_{101} and TE_{102} resonance of (10), based on half wavelength resonance. The P1, P2, and P3 mean the $\mathrm{TE}_{10\delta}$ resonant points by

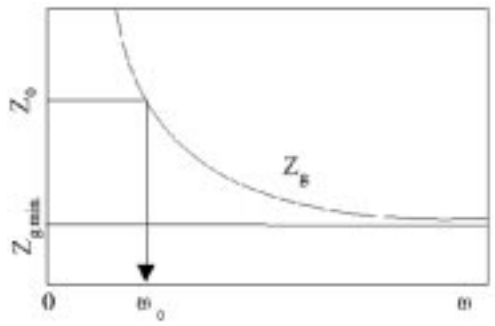

Fig. 4. The center frequency of $\mathrm{TE}_{10\delta}$ mode and its restriction.

(14), and the electrical lengths are dependent on the load Y_0. One limit value of the resonant frequencies of (14) is the cutoff frequency. As the load Y_0 is closer to zero, the resonant frequency approaches to the waveguide cutoff frequency f_c and the electrical length is closer to zero as in (14) and Fig. 3. According to the load value, the half wavelength resonance can be changed from parallel to series resonance or reverse as the case of $Y_0 = 1/25$. If the load Y_0 is much higher than maximum Y_g, the OEF will be seen like a short circuit and $\mathrm{TE}_{10\delta}$ will be disappeared as the case of $Y_0 = 1/25$ in Fig. 3. In order to make this limitation clear, a real condition is forced to the square root term of (14) and (16) is obtainedas follows:

$$\frac{a}{b} > Y_0 \eta_0 \frac{d_z}{\sqrt{\varepsilon_r}}. \tag{16}$$

Equation (16) represents the relationship between resonator dimensions, dielectric constant and load impedance for the $\mathrm{TE}_{10\delta}$ resonance. It implies that with high permittivity dielectric material such as ceramics, $\mathrm{TE}_{10\delta}$ resonator can be easily formed. (16) can be also written as (17) equivalently. It means that the load impedance has to be larger than the lower limit of the waveguide characteristic impedance, $Z_{g\min}$, which can be seen graphically from Fig. 4

$$Z_{g\min.} = Z_g|_{\omega\to\infty} = \eta d_z < Z_0, \tag{17}$$

where $\eta = \sqrt{\mu/\varepsilon_r\varepsilon_0}$, $Z_g = 1/Y_g$, and $Z_0 = 1/Y_0$.

In Fig. 3, though $Z_0\,(=25)$ is also larger than $Z_{g\min}\,(=17.24)$, the $\mathrm{TE}_{10\delta}$ resonant frequency (or electrical length) by (14) is so high (or large) that it cannot be seen in the frequency range of the figure. The resonant frequency of (14) is not always below that of half wavelength resonance (TE_{101}). In practice, any frequency can be chosen as the resonant frequency, but if a frequency below TE_{101} resonance is chosen, the slope parameter value by (15) is not so small and is proper to design a bandpass filter (BPF)that has narrow or moderate bandwidth.

B. OEF Characteristics of a WGS

If the effect of an OEF is not negligible, we should consider additional susceptance B_a at both OEFs of the resonator. Lets consider a rectangular waveguide resonator filled with ZST series ceramics of $\varepsilon_r = 38$. The dimensions $a \times b \times d$ are 20.0 × 5.0 × 10.0 [see Fig. 1(a)].

Several possible resonator configurations are given in Figs. 5 and 6, according to the OEF conditions of the resonators. The

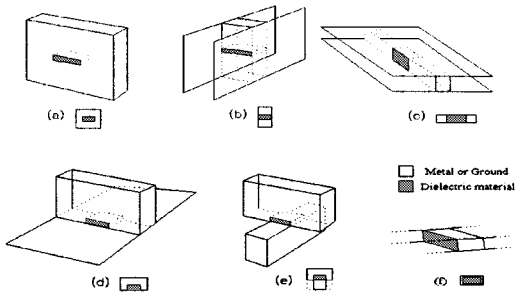

Fig. 5. Type I resonators.

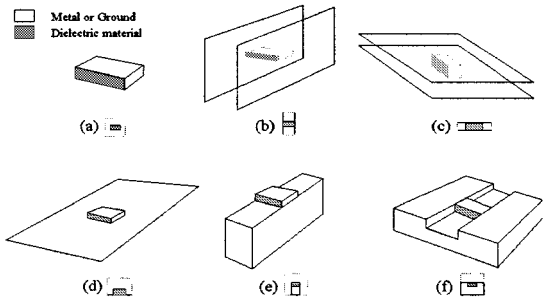

Fig. 6. Type II resonators.

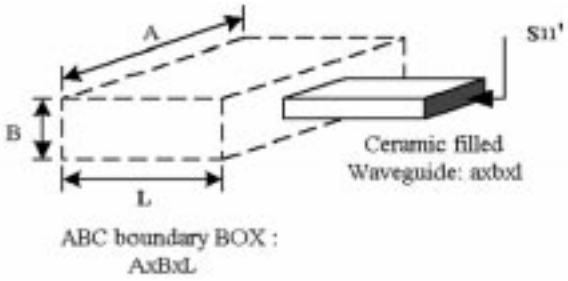

Fig. 7. ABC boundary BOX (see text also).

white parts of the figures represent ground or metal parts and the shaded parts are dielectric materials. All of the Type I configurations work as rectangular waveguide mode resonators. Type II resonators can work as a mixed rectangular waveguide mode with microstrip mode except Type II-(c). Type II-(d) was reported in TEM dielectric mode filter structure [11], and as "a SMD type partially metallized rectangular dielectric resonator" [17].

The additional susceptance B_a values of each OEF are inspected with HFSS, according to the OEF conditions. First, the one port scattering parameter S'_{11} was obtained by applying ABC (absorbing boundary condition) to the open end as in Fig. 7. The dimensions $A \times B \times L$ of ABC box are 200 × 80 × 100 (mm), if any ground does not limit the dimensions. The dimensions are chosen such that the solution could converge, and then the dimensions could be larger than 0.3λ of the free-space wavelength [12]. The parameter S'_{11} was de-embedded in order to remove the length l of the dielectric-filled waveguide in Fig. 7. Then the resultant S_{11} was converted into admittance parameter, Y_{11}, to determine the additional susceptance B_a using (18)

$$Y_{11} = Y_g \frac{1 - S_{11}}{1 + S_{11}} \quad B_a = \mathrm{Im}[Y_{11}]. \tag{18}$$

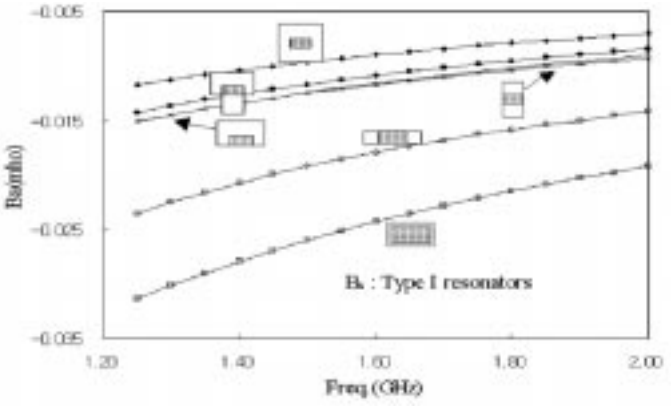

Fig. 8. B_a values of Type I resonators.

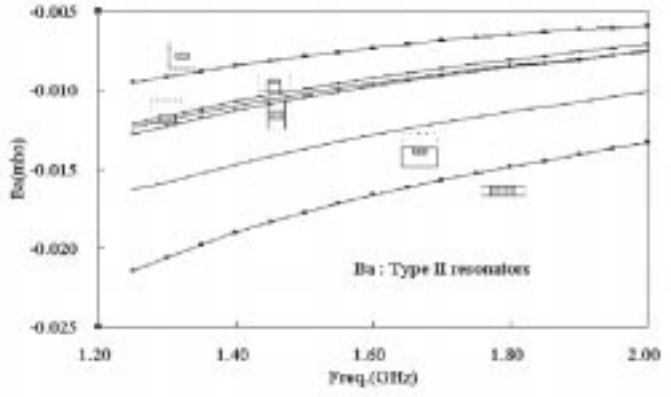

Fig. 9. B_a values of Type II resonators.

The calculated B_a values of Type I and Type II resonators are shown in Figs. 8 and 9, respectively. The B_a values are all negative. It means that the open ends give inductive characteristics equivalently. The OEF gives lower inductive value, as the ground planes are wider.

C. $\mathrm{TE}_{10\delta}$ Resonant Frequency

Once B_a value is determined the resonant frequency of a resonator can be calculated by (3) and (5). To verify the calculations by experiment we measured the resonant frequencies under loose coupling condition. One measured result is shown in Fig. 10 for Type II-(e) resonator with $\varepsilon_r = 38.4$, $a = 20.0$, $b = 5.0$ and $d = 10.0$ mm. Each marker pointed to $\mathrm{TE}_{10\delta}$, TE_{101}, TE_{102}, and $\mathrm{TE}_{11\delta}$ mode peaks, respectively. We assumed infinite Z_o, which is practical assumption because Z_0 is so high that it could not change the resonant frequency under loose coupling condition. The comparison of measured and calculated mode data are also given on Table I. The differences of the two corresponding frequencies are all under 2%. The errors are partially caused by the roughness of metallized wall which gives nonzero gap between the resonator and ground plane. It was more than several hundred micrometers sometimes according to metallizing condition. Hence, the B_a by the OEF could be increased and the resonant frequency could be decreased in measuring process.

Another comparison is given in Table II for a resonator of Type II-(d) with $\varepsilon_r = 94$, $a = 9.0$, $b = 1.9$, $d = 10.5$. In this case, the resonator length d is so long that the resonant frequency of TE_{101} is closer to that of $\mathrm{TE}_{10\delta}$.

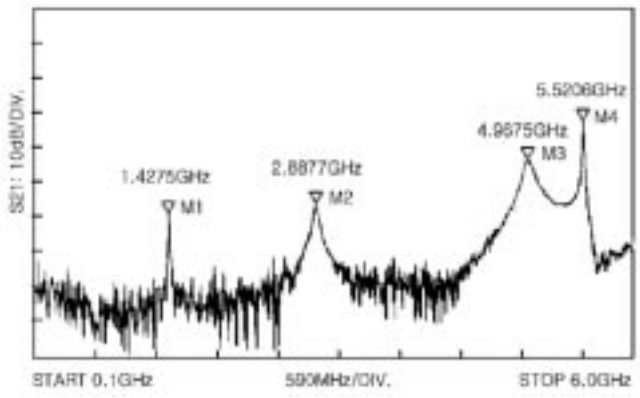

Fig. 10. Measured lowest four-poles for a type II-(e) resonator; $M1 = \mathrm{TE}_{10\delta}$, $M2 = \mathrm{TE}_{101}$, $M3 = \mathrm{TE}_{102}$, $M4 = \mathrm{TE}_{11\delta}$.

TABLE I
COMPARISON OF MEASURED AND CALCULATED RESONANT FREQUENCIES. USED RESONATOR: $\varepsilon_r = 38.4$, $a = 20.0$, $b = 5.0$, $d = 10.0$ mm AND TYPE II-(e). SEE ALSO FIG. 10 AND TEXT

Modes	Calculated (GHz)	Measured (GHz)	Error ratio (%)
$\mathrm{TE}_{10\delta}$	1.449	1.424	-1.73
TE_{101}	2.907	2.888	-0.65
TE_{102}	5.000	4.968	-0.64
$\mathrm{TE}_{11\delta}$	5.600	5.521	-1.41

TABLE II
COMPARISON OF MEASURED AND CALCULATED RESONANT FREQUENCIES. USED RESONATOR: $\varepsilon_r = 94$, $a = 9.0$, $b = 1.9$, $d = 10.5$ (mm), AND TYPE II-(d)

Modes	Calculated (GHz)	Measured (GHz)	Error ratio (%)
$\mathrm{TE}_{10\delta}$	1.834	1.8062	-1.52
TE_{101}	2.449	2.4156	-1.36
$\mathrm{TE}_{20\delta}$	3.495	3.4783	-0.48

According to the length "d" and the height "b" of a resonator, the higher order modes, TE_{101}, TE_{102}, and $\mathrm{TE}_{11\delta}$ could be located on much higher frequencies as it can be read in (10) and (14). In other words, the electrical length of the $\mathrm{TE}_{10\delta}$ resonator can be chosen arbitrary using equation (3) and the data in Figs. 8 or 9, because the susceptance B_a value is changed not by the resonator length but by the frequency. In practice, the electrical length 0.X radian can also work as a resonator as in the Fig. 11. Using short-length resonator the spurious response by TE_{101} modes could be avoided.

In Table III, the calculated and measured resonant frequencies of the 12 resonators in Figs. 5 and 6 were compared each other. The same resonator with $\varepsilon_r = 38.4$, $a = 20.0$, $b = 5.0$, and $d = 10.0$ mm was used. All the measured frequencies agree well with calculated data as the above examples. The effect of OEF is to increase frequencies to all resonance, because all of the B_as are inductive value as shown in Figs. 8 and 9.

A top view of H-field distribution of a $\mathrm{TE}_{10\delta}$ resonance is shown in Fig. 12. This was re-drawn from HFSS field data. The PMW is shifted into the interior of resonator as Kundu [4] has mentioned. For the $\mathrm{TE}_{10\delta}$ mode, very short resonator length

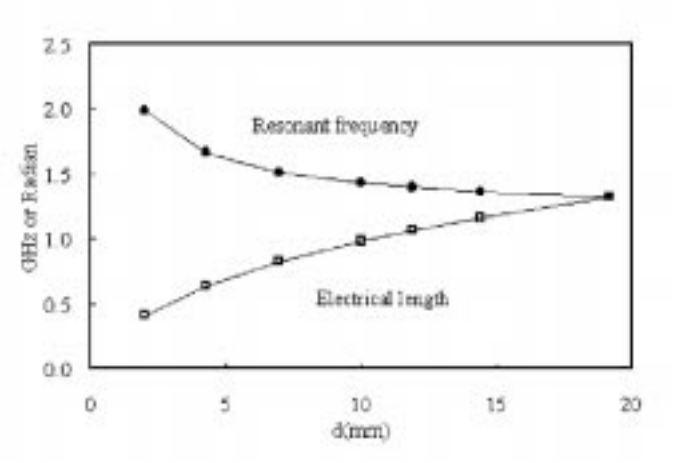

Fig. 11. Electrical length and $TE_{10\delta}$ resonant frequencies: Type II-(e) resonator with $\varepsilon_r = 38.4$, $a = 20.0$ mm, $b = 5.0$ mm, (3), (4), and the data in Fig. 9 are used in calculation.

TABLE III
RESONANT FREQUENCY COMPARISON OF 12 TYPES OF $TE_{10\delta}$ RESONATORS; A RESONATOR WITH $\varepsilon_r = 38.4$, $a = 20.0$, $b = 5.0$ AND $d = 10.0$ (mm), EQUATION (3) AND THE DATE IN FIGS. 8 AND 9 WERE USED

Resonator	Type-I (GHz)		Type-II(GHz)	
	Calculated	Measured	Calculated	Measured
(a)	1.449	1.424	1.406	1.389
(b)	1.497	1.476	1.454	1.433
(c)	1.608	1.592	1.588	1.588
(d)	1.496	1.478	1.459	1.432
(e)	1.482	1.468	1.449	1.429
(f)	1.702	-	1.519	1.503

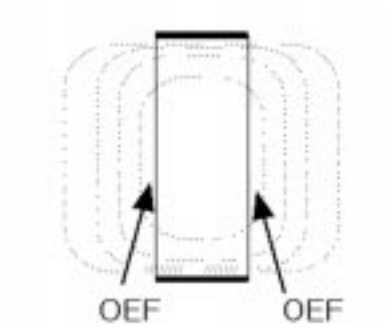

Fig. 12. Top view of $TE_{10\delta}$ (H-field).

can be also chosen, because the PMW is at the center of the resonator.

D. The Quality Factors

In this type of resonators, at least, there are three kinds of losses such as conductor, dielectric, and radiation loss. Those are represented in terms of Q_c, Q_d, and Q_r, respectively. Lets consider that a dielectric-filled WGS of length d is extended with empty infinite waveguide [Type I-(f)], as in Fig. 13. The field distributions [5] inside and outside of the section are given by (19)–(24). The TE_{10} mode is supposed to be in the section. The $\mathbf{E}$, $\mathbf{H}$ and $\mathbf{E}'$, $\mathbf{H}'$ represent the electric and magnetic fields

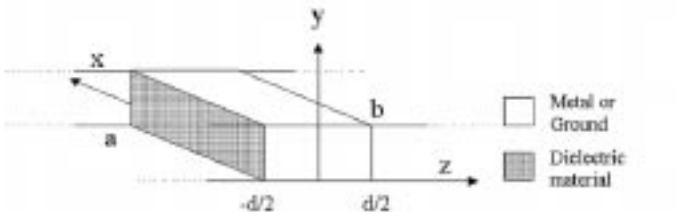

Fig. 13. Coordination system for Type I (f) resonator.

inside and outside of the resonator (dielectric-filled WGS), respectively

$$E_y = E_0 \sin\frac{\pi x}{a}\cos\beta z \tag{19}$$

$$H_x = -j\frac{E_0\beta}{\omega\mu}\sin\frac{\pi x}{a}\sin\beta z \tag{20}$$

$$H_z = j\frac{E_0}{\omega\mu}\left(\frac{\pi}{a}\right)\cos\frac{\pi x}{a}\cos\beta z \tag{21}$$

$$E'_y = E_0 \sin\frac{\pi x}{a}\cos\frac{\beta d}{2}\,e^{\alpha(z-d/2)} \tag{22}$$

$$H'_x = j\frac{E_0\alpha}{\omega\mu}\sin\frac{\pi x}{a}\sin\frac{\beta d}{2}\,e^{-\alpha(z-d/2)} \tag{23}$$

$$H'_z = j\frac{E_0}{\omega\mu}\left(\frac{\pi}{a}\right)\cos\frac{\pi x}{a}\cos\frac{\beta d}{2}\,e^{-\alpha(z-d/2)}. \tag{24}$$

The quality factor due to conductor loss, Q_c can be represented as a ratio of stored energy, P_{EM}, and conductor loss, P_c, from the finite conductivity of the conductor of the resonator. The stored energy terms of the E-field (P_e, P'_e) and H-field (P_m, P'_m) are calculated as (25)–(28)

$$P_e = \frac{\varepsilon}{4}\int_v E_y\cdot E_y^*\,dv = \varepsilon\frac{ab}{16}E_0^2\left(d+\frac{\sin\beta d}{\beta}\right) \tag{25}$$

$$P_m = \frac{\mu}{4}\int_v (H_x\cdot H_x^* + H_z\cdot H_z^*)\,dv = \frac{\varepsilon E_0^2}{16}ab\left(d+\frac{K_c^2-\beta^2}{K^2}\frac{\sin\beta d}{\beta}\right) \tag{26}$$

$$P'_e = 2\times\frac{\varepsilon_0}{4}\int_{v'} E'_y\cdot E'^*_y\,dv' = \frac{\varepsilon_0}{\alpha}\frac{ab}{8}E_0^2\cos^2\frac{\beta d}{2} \tag{27}$$

$$P'_m = 2\times\frac{\mu}{4}\int_{v'}(H'_x\cdot H'^*_x + H'_z\cdot H'^*_z)\,dv' = \frac{\mu}{\alpha}\frac{ab}{8}E_0^2\left[\left(\frac{\alpha}{\omega\mu}\right)^2\sin^2\frac{\beta d}{2}+\left(\frac{K_c}{\omega\mu}\right)^2\cos^2\frac{\beta d}{2}\right] \tag{28}$$

$$P_{EM} = P_e + P'_e + P_m + P'_m \tag{29}$$

where E^* and H^* are the conjugate complexes of the E and H, respectively.

The conductor loss P_c and the quality factor Q_c can be calculated as follows:

$$P_c = \frac{R_s}{2}\int_s J_s\cdot J_s^*\,ds = \varepsilon\frac{ab}{8}E_0^2\left[d+\frac{\alpha}{K^2}+\frac{1+\cos\beta d}{\varepsilon_r\alpha}+\left(\frac{K_c}{K}\right)^2\frac{\sin\beta d}{\beta}\right] \tag{30}$$

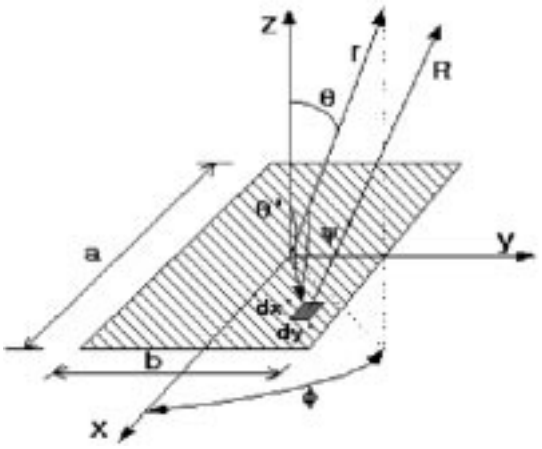

Fig. 14. Rectangular aperture for radiation of OEF.

where $J_s = n \times H$

$$Q_C = \frac{\omega_0 P_{EM}}{P_c} = \frac{\eta\varepsilon ab}{4R_S} \frac{\left[d + \frac{\alpha}{K^2} + \frac{1+\cos\beta d}{\varepsilon_r \alpha} + \left(\frac{K_c}{K}\right)^2 \frac{\sin\beta d}{\beta}\right]}{\left[\left(\frac{K_c}{K}\right)^2 \left(b+\frac{a}{2}\right)\left(d+\frac{\sin\beta z}{\beta}\right) + \left(\frac{\beta}{K}\right)^2 \frac{a}{2}\left(d-\frac{\sin\beta z}{\beta}\right)\right]} \tag{31}$$

where $R_s = \sqrt{\omega\mu/2\sigma}$, $\eta = \sqrt{\mu/\varepsilon}$.

The dielectric quality factor, Q_d is calculated simply from Qf, value as follows:

$$Q_d = \frac{Qf}{f_0} \quad Qf = Q_d \times f \text{ GHz}. \tag{32}$$

In order to consider radiation loss from the OEF, Konishi [1] derived P_r and Q_r by replacing the electric field of the OEF by magnetic current M_s

$$P_r = \frac{8}{3\pi} \frac{a^2 b^2}{\lambda_0^2} \frac{E_0^2}{\eta_0} \tag{33}$$

$$Q_r = \varepsilon_r \frac{3\pi^2}{32} \frac{d\lambda_0}{ab} \tag{34}$$

where P_r is the radiated power, and Q_r is the radiation Q factor, λ_0 is the free-space wavelength, and η_0 is the free-space intrinsic impedance. He assumed the OEF as a PMW. But this assumption sometimes gives big difference between measured and calculated Q_rs. In practice, the ε_r is not infinite (normally, less than 100), the tangential component of the magnetic field exists at the OEF, and some energy can be stored around outside of the OEF. This magnetic field causes an effective electric current source J_s at the OEF and additional loss [4], [5].

Let us consider the coordination system shown in Fig. 14, used to derive the radiation loss at the OEF of the resonator. The tangential components of the electromagnetic fields at the OEF are E_y and H_x. For the simplicity of the problem, if these fields are distributed uniformly with keeping conservation of the total power, the tangential components $\mathbf{E_a}$ and $\mathbf{H_a}$ are given by (35) and (36) from (22) and (23), respectively. If the distance $|\mathbf{r}|$ to the observer is large enough, this approximation become appropriate

$$E_a = \frac{E_0}{\sqrt{2}} \cos\frac{\beta d}{2} \vec{a}_y \tag{35}$$

$$H_a = \frac{j}{\sqrt{2}} \frac{E_0 \alpha}{\omega\mu} \sin\frac{\beta d}{2} (-\vec{a}_x). \tag{36}$$

By the equivalence principle, the equivalent current densities J_s and M_s are obtained as follows:

$$J_s = \vec{n} \times H_a = -j \frac{E_0 \alpha}{\sqrt{2}\omega\mu} \sin\frac{\beta d}{2} \vec{a}_y \tag{37}$$

$$M_s = -\vec{n} \times E_a = \frac{E_0}{\sqrt{2}} \cos\frac{\beta d}{2} \vec{a}_x. \tag{38}$$

After far field ($kr \gg 1$) analysis, the radiated power P_r from OEF is obtained as (40)

$$E_\theta = j \frac{kre^{-jkr}}{4\pi r} ab \sin\phi (E_{ay} + \eta_0 H_{ax} \cos\theta) \frac{\sin X}{X} \frac{\sin Y}{Y} \tag{39}$$

$$P_r = \frac{1}{\eta_0} \int_\phi \int_\theta |E_\theta|^2 r^2 \sin\theta \, d\theta \, d\phi = \frac{1}{\eta_0} \int_\phi \int_\theta \{E_{ay}^2 + (\eta_0 |H_{ax}| \cos\theta)^2\} \cdot \sin\theta \sin^2\phi \, d\theta \, d\phi \left(\frac{kab}{4\pi} \frac{\sin X}{X} \frac{\sin Y}{Y}\right)^2 d\theta \, d\phi \tag{40}$$

where

$$E_{ay} = \frac{E_0}{\sqrt{2}} \cos\frac{\beta d}{2} \quad H_{ax} = \frac{j}{\sqrt{2}} \frac{E_0 \alpha}{\omega\mu} \sin\frac{\beta d}{2}$$

and

$$X = \frac{ka}{2} \sin\theta \cos\phi \quad Y = \frac{kb}{2} \sin\theta \sin\phi.$$

The radiation quality factor Q_r is then calculated as follows:

$$Q_r = \omega_0 \frac{P_{EM}}{P_r}. \tag{41}$$

The unloaded quality factor can also be calculated using following equation:

$$Q_u = (Q_c^{-1} + Q_d^{-1} + Q_r^{-1})^{-1}. \tag{42}$$

Using the above equations, we calculated quality factors of the resonator [$a \times b \times d = 20 \times 5 \times 10$ (mm), $\varepsilon_r = 38.4$]. The quality factors versus the resonators length d is plotted in Fig. 15. The measured Q_u of Type II-(e) is also shown in the same figure. The used dielectric material is a ZST (Zr–Sn–Ta) series ceramic with Qf value of 20 000. The thickness of the silver coating was five to ten times the skin depth (1–2 μm). The resultant conductivity of the silver coating is 60% to 70% of that of the pure Ag [1], [5]. We used 60% of the conductivity. As the length of the resonator is decreased, the radiation loss is increased and become the dominant factor in the total unloaded quality factor, Q_u.

E. $TE_{10\delta}$ *Resonator With Electrodes at Both Opposite Sides*

When we use a resonator in practice, coupling ports to the input and the output are needed. Gonishi [1] has suggested

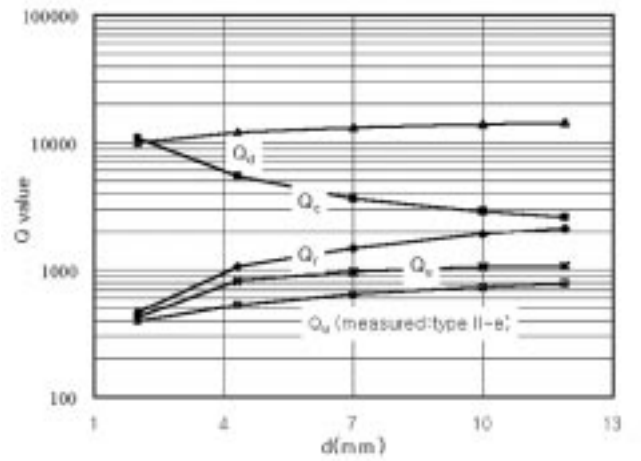

Fig. 15. Calculated and measured Q-factors of the resonator. $a \times b \times d = 20 \times 5 \times d$ (mm) and $\varepsilon_r = 38.4$.

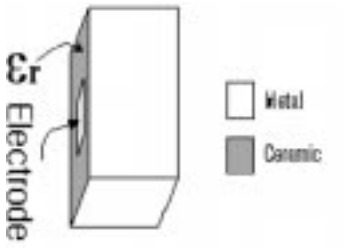

Fig. 16. Electrode structure at OEFs.

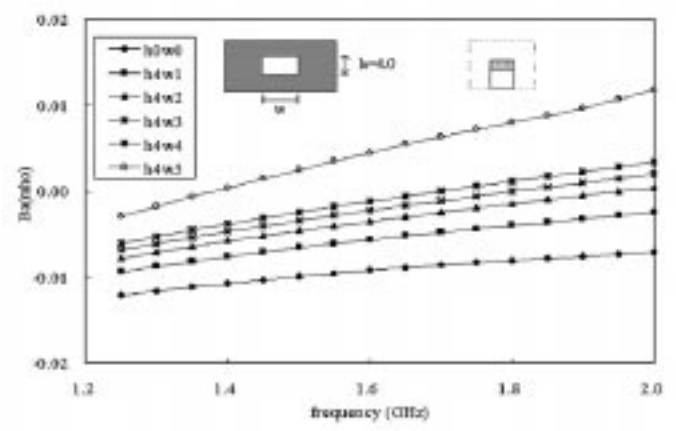

Fig. 17. Calculated B_a values according to electrode size ($h0w0$ means $h = 0$ mm and $w = 0$ mm). The used resonator: $20 \times 5 \times 10$ (mm), $\varepsilon_r = 38.4$.

metal-coated electrode on the open face of the ceramic resonator, previously. We can use the structure for these resonators as in Fig. 16. The electrodes are formed on the center of both OEFs and the dimensions are given as height "h" and width "w" in millimeter. For example, $h4w1$ means that the height is 4 mm and the width is 1 mm.

In this case, the change of the load B_a by the electrode should be considered. According to various electrode dimensions, the width "w" and the height "h," the calculated values are presented in Fig. 17, after the same analysis using HFSS. As the dimensions of the electrode increase, the B_a value also increase. This gives the result of a decreasing resonant frequency as in Fig. 18.

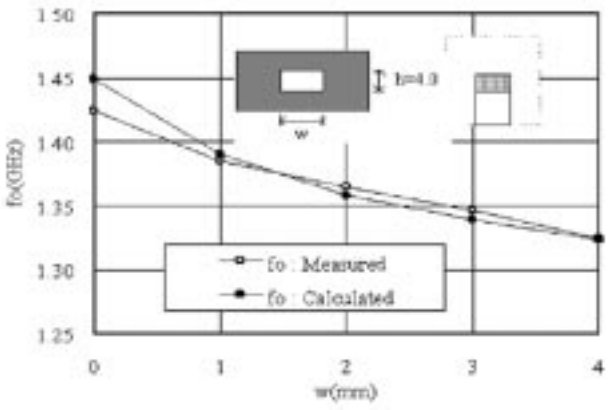

Fig. 18. Frequency changes according to width w of the electrode. The used resonator: $20 \times 5 \times 10$ (mm), $\varepsilon_r = 38.4$.

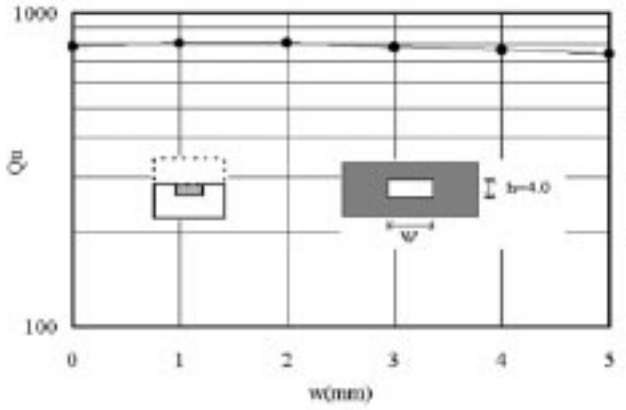

Fig. 19. Measured Q factor versus electrode size when $h = 4.0$ mm: $a \times b \times d = 20 \times 5 \times 10$ (mm), $\varepsilon_r = 38.4$.

When the width of the electrode, w, is about 2.0 mm, the quality factor is maximum. However, the electrode of the OEF is not highly affective to the quality factor as shown in Fig. 19.

III. Bandpass Filter Applications

As was discussed in the previous section, when B_a is zero, the resonant frequency is given by (14). In order to take an example for this resonance, we tried to design a waveguide BPF with two kinds of dielectric materials. The structure is shown in Fig. 20. For the resonator parts a dielectric material with relative dielectric constant of 2.0 is used. The other parts, air and the material of relative dielectric constant of 6.0, consist the inverters as the inverter structure of Fig. 21. The resonant frequency and the slope parameter of the resonator are calculated directly by using (14) and (15).

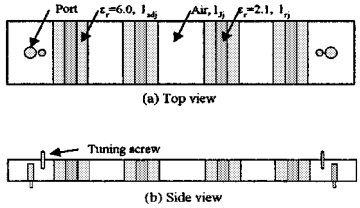

Fig. 20. A crosscut of the four-pole BPF used frequency dependency of WG characteristic impedance.

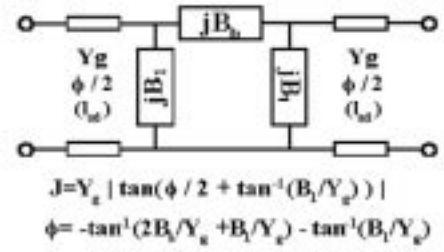

Fig. 21. J inverter for the BPF of Fig. 32.

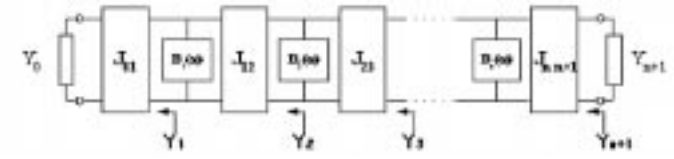

Fig. 22. A BPF with admittance inverters and the definition of Y_j.

We used the general BPF design method where the inverter concept is used as in Fig. 21. The design equations are well known as (43)–(45) [13]

$$J_{01} = \sqrt{\frac{Y_0 W \bar{b}_1}{\omega_1' g_0 g_1}} \tag{43}$$

$$J_{jj+1} = \frac{W}{\omega_1'}\sqrt{\frac{\bar{b}_j \bar{b}_{j+1}}{g_j g_{j+1}}}, \qquad \text{where } j = 1, 2, 3, \ldots, n. \tag{44}$$

$$J_{nn+1} = \sqrt{\frac{Y_{n+1} W \bar{b}_n}{\omega_1' g_n g_{n+1}}} \tag{45}$$

where W is the fractional bandwidth and g_j is the lowpass prototype element value.

Differently from lumped *LC* resonator, the center frequency and the slope parameter of the waveguide resonator can be changed by load levels, as was discussed in the previous section. The loads of each resonator have to be involved into the design procedure, especially, in designing a BPF of wide bandwidth. For this reason, an additional condition should be considered as (46). The Y_j is the admittance shown in Fig. 22 is as follows:

$$Y_j = \frac{J_{jj-1}}{Y_{j-1}}, \qquad \text{where } j = 0, 1, 2, \ldots, n+1. \tag{46}$$

With the resonator parameters calculated by equations of previous sections and these design equations, we obtained the BPF

TABLE IV
DESIGN VALUES OF THE BPF IN FIG. 20

Filter Spec.		N=4, fo=5.173GHz, BW=230MHz, ripple =0.01		
Resonator Spec.		a=20mm, b=5mm, slope parameter =0.00193		
		resonator	inverter(Φ/2)	inverter(B_x)
ε_r		2.1	6.0	1.0
Length (mm)	1st	l_1=1.6	l_{ad1}=3.12	l_{J1}= 6.36
	2nd	l_2=1.6	l_{ad2}=2.31	l_{J2}=19.16
	3rd	l_3=1.6	l_{ad3}=2.29	l_{J3}=21.94
	4th	l_4=1.6	l_{ad4}=2.31	l_{J4}=19.16
	5th	-	l_{ad5}=3.12	l_{J5}= 6.36

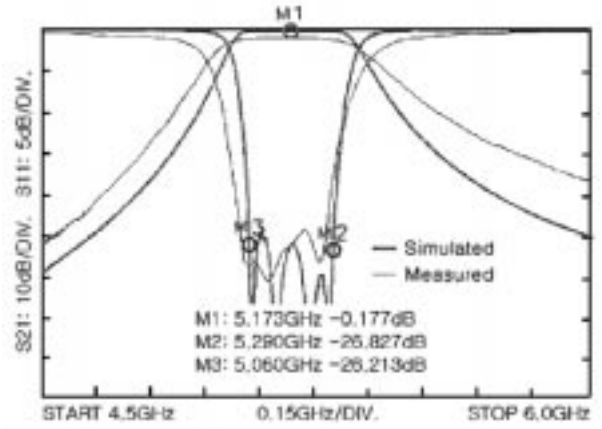

Fig. 23. Frequency responses of the BPF on Table IV and in Fig. 20.

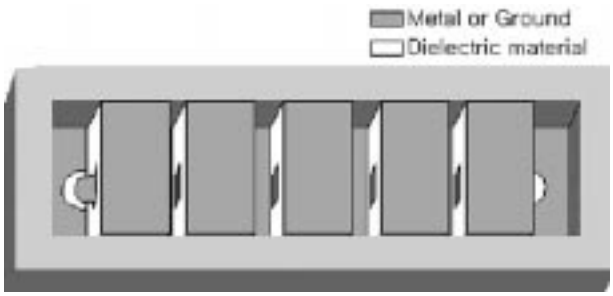

Fig. 24. Five-pole BPF structure using Type II-(f) resonators (not scaled).

dimensions as on Table IV. The frequency dependent property of the Inverter [14] was also considered.

The simulated and measured frequency responses for the four-pole BPF are given in Fig. 23. They agree well with the design specifications such as center frequency, bandwidth, and passband ripple. The difference between measured and simulated characteristics is mainly caused by the unwanted gaps between dielectric layers of resonators and inverters.

Using Type II-(f) resonators, the BPF that upside is opened was designed as another example. The filter structure is given in Fig. 24.

The design values and frequency response are also given in Table V and in Fig. 28. In the Table V "$-\delta$" represents a small decreasing of the electrode dimension after frequency tuning process. The coupling coefficient concept [13]–[16] was used in the design procedure. The bandwidth of the filter is a function

TABLE V
DESIGN VALUES OF 4-POLE BPF IN FIG. 24

Filter Spec.	n=5, f0=1.385GHz, BW=3%(40.2MHz), Ripple=0.01					
Resonator	ε_r=38.4, a=20mm, b=5mm, d=10mm					
Index i j	0 1	1 2	2 3	3 4	4 5	5 6
Coupling k	0.179	0.030	0.020	0.020	0.030	0.179
D(mm)	-	8.8	10.6	10.6	8.8	-
h,w(mm)	4, 5	4-δ,5	4-δ,5	4-δ,5	4-δ,5	4, 3

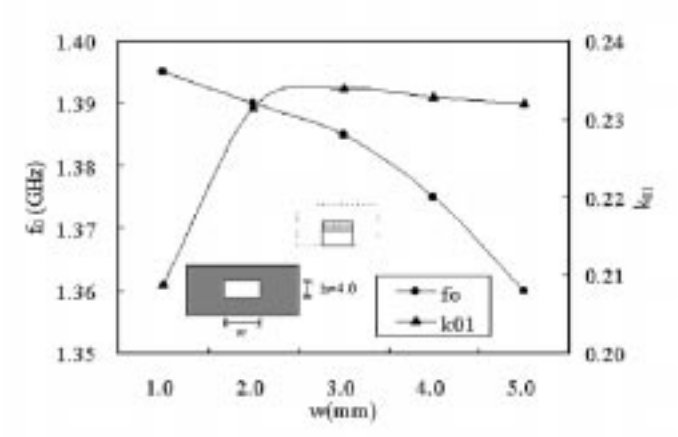

Fig. 25. Measured f_0 and k_{01} values according to width w of electrode.

of inverters and slope parameters of the resonators used in the BPF. The coupling coefficients k_{01}, k_{ij} can be defined as in (47) and (48)

$$k_{01} = \frac{1}{\sqrt{Q_e}} = \frac{J_{01}}{\sqrt{Y_0 \bar{b}_1}} = \sqrt{\frac{W}{g_0 g_1 \omega_1'}} \tag{47}$$

$$k_{ij}|_{j=1\cdots n-1} = \frac{J_{jj+1}}{\sqrt{\bar{b}_j \bar{b}_{j+1}}} = \frac{W}{\omega_1' \sqrt{g_j g_{j+1}}}. \tag{48}$$

The coupling coefficient k_{01} can be calculated by measuring external quality factor Q_e or fractional bandwidth, W, when a resonator is coupled to an external circuit that has admittance Y_0. The inter-resonator coupling coefficient k_{ij} is also easily determined by measuring fractional bandwidth W or peak frequencies f_1 and f_2 under loose coupling condition of two identical resonators, and (49) [15], [16]

$$k_{ij}|_{j=1,\ldots,n-1} = \frac{f_2^2 - f_1^2}{f_2^2 + f_1^2} \approx \frac{W}{\sqrt{2}}. \tag{49}$$

Some experimental results of the coupling coefficients are given in Figs. 25–27. The dimensions $a \times b \times d$ are $20 \times 5 \times 10$ (mm) and the relative permittivity ε_r is 38.4 in the figures. The electrode size is not so critical to the coupling coefficient k_{01} values if it is above some value ($w = 2.0$ mm), differently from resonant frequencies, as shown in Fig. 25. In Fig. 26, we can see that the inter-resonators coupling coefficient k_{ij} is not sensitive to the electrode dimensions "w" and "h." Hence, we can design the BPF with the data in Fig. 27. The dimension D is the distance between two coupled resonators as in Figs. 26 or 27.

Using Type II-(d) resonators with a material of relative dielectric constant ε_r of 94, and dimension $a \times b \times d$ of $9.5 \times 1.5 \times$ 1.8 mm, a four-pole BPF with f_0 of 2.0 GHz, BW of 100 MHz was designed. In order to reduce the spurious response, the short length was chosen. The filter structure is given in Fig. 29, with the design values in Table VI. The frequency response is given in Fig. 30. In Fig. 31, the higher TE_{10X} modes are effectively suppressed; only $\mathrm{TE}_{10\delta}$, $\mathrm{TE}_{20\delta}$, $\mathrm{TE}_{30\delta}$ modes appear. The $\mathrm{TE}_{20\delta}$ mode was also suppressed below -36 dB. Because the excitation at the port electrode is symmetric along the dimension "a," the electromagnetic field of $\mathrm{TE}_{20\delta}$ mode, which is odd function shape, is hardly to be formed.

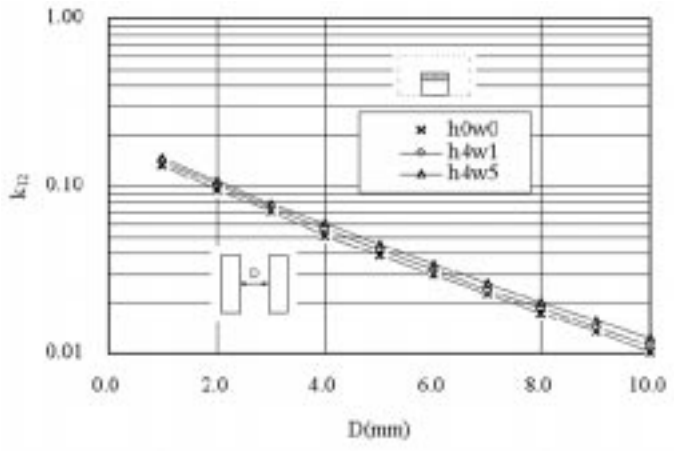

Fig. 26. Measured coupling coefficient k_{12}.

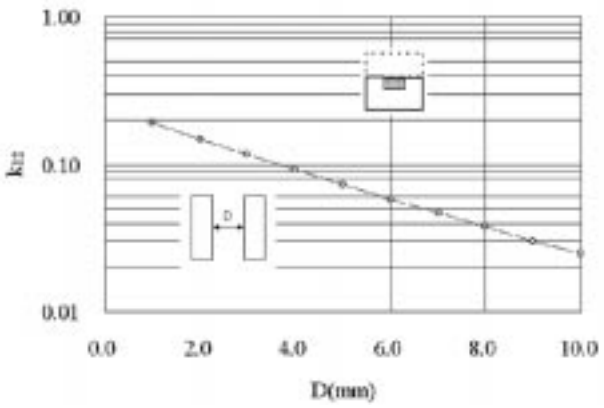

Fig. 27. Measured coupling coefficient k_{12}. D is the coupling distance.

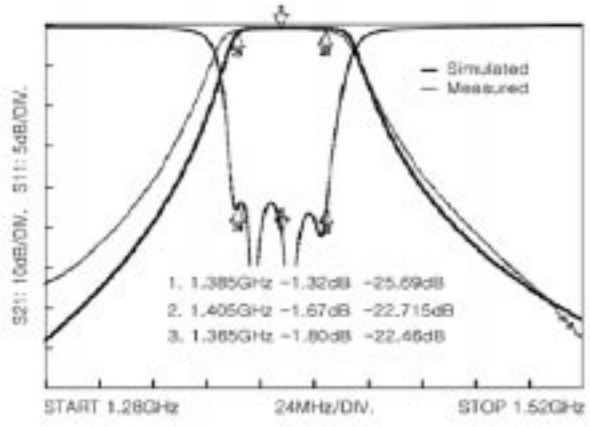

Fig. 28. Frequency responses of the five-pole BPF in Fig. 24 and on Table V.

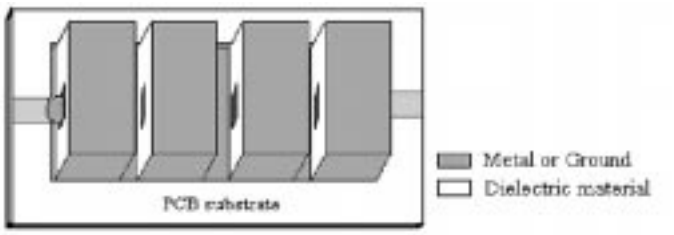

Fig. 29. Four-pole BPF structure with Type II-(d): $\varepsilon_r = 94$, and dimensions $a = 9.5$ mm, $b = 1.5$ mm, and $d = 1.8$ mm. (Not scaled.)

TABLE VI
DESIGN VALUES OF 4-POLE BPF IN FIG. 29

Filter Spec.	n=4, f_0=2.0GHz, BW=100MHz, Ripple=0.05dB				
Resonator	ε_r=94, a=9.5mm, b=1.5mm, d=1.8mm				
Index i j	0 1	1 2	2 3	3 4	4 5
Coupling k	0.228	0.0448	0.0346	0.0448	0.228
Coupling D (mm)	-	2.9	3.3	2.9	-

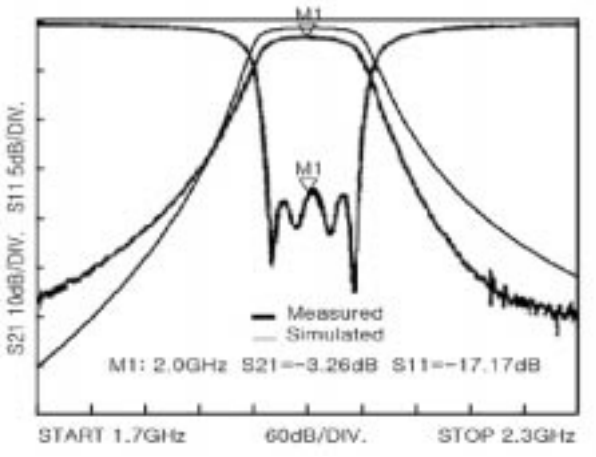

Fig. 30. Frequency responses of the four-pole BPF in Fig. 29 and in Table VI.

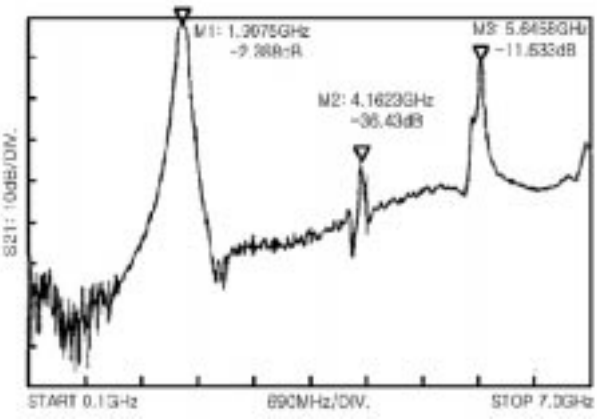

Fig. 31. Measured spurious response of the four-pole BPF in Fig. 29 and on Table VI.

The design values are given for the four pole BPF with Type II-(d) resonators in Table VI. The coupling D represents the physical distance between two adjacent resonators.

To inspect the effect of a housing, we prepared some metal cases larger than a two-pole filter in which two resonators are coupled by a distance, $D = 5$ mm. DD means the distance from the two-pole filter to any nearest case walls as shown in Fig. 32. DD is not sensitive from 5 mm for coupling coefficient, and from 10 mm for resonant frequency as in Fig. 32. Type II-(d) resonators with $\varepsilon_r = 38.4$, $a = 20.0$, $b = 5.0$ and $d = 10.0$ (mm) were used. As the resonator dimension "b" is decreased, the effect of a housing also decreased by other experiments. This data is useful for not only when the resonator or filter is packed but also when it is used directly on PCB as an SMD.

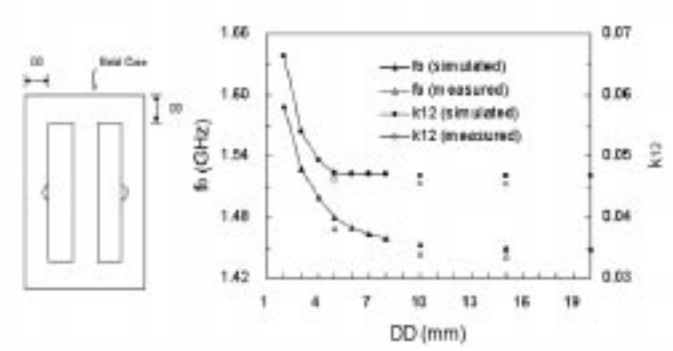

Fig. 32. The effect of a housing; coupling coefficients and resonant frequencies versus gap, DD. The all distances from nearest case walls are all the same DD.

IV. CONCLUSION

New rectangular-waveguide-type $\mathrm{TE}_{10\delta}$ dielectric resonators were investigated. The calculated and measured resonant frequencies agree well with each other, and depend strongly on the width "a" of the WGS and loosely on the length and the height. Hence, the dimensions of the resonator can be chosen almost arbitrarily except the width "a." The resonator could be also designed as a planar SMD device because the resonant frequency is hardly changed by a variation of the height "b" of the WGS. The proposed BPF shows highly reduced spurious up to three times the center frequency. Newly calculated quality factors including radiation Q agree well with experimental results. The effect of a housing was also discussed. This data could be also used as a guideline of spacing from other devices when this resonator or filter is directly used on a system PCB without individual housing.

ACKNOWLEDGMENT

The authors would like to thank Prof. I. S. Chang of Sogang University, South Korea, and Dr. P. K. Kim of Amotech Company, for assistance and Prof. K. A. Zaki, University of Maryland at College Park (UMCP), for helpful comments.

REFERENCES

[1] Y. Konishi, "Novel dielectric waveguide components microwave applications of new ceramic materials," *Proc. IEEE*, vol. 79, no. 6, pp. 726–740, June 1991.
[2] K. Wakino, T. Nishikawa, and Y. Ishikawa, "Miniaturization technologies of dielectric resonator filters for mobile communications," *IEEE Trans. Microwave Theory Tech.*, vol. 42, pp. 1295–1300, July 1994.
[3] ——, "Miniaturized diplexer for land mobile communication using high dielectric ceramics," in *IEEE MTT-S Int. Microwave Symp. Dig.*, vol. 81-1, 1981, pp. 185–187.

[4] A. C. Kundu and I. Awai, "Resonant frequency and quality factors of a silver-coated $\lambda/4$ dielectric waveguide resonator," *IEEE Trans. Microwave Theory Tech.*, vol. 46, pp. 1124–1131, Aug. 1998.
[5] H. Kubo and H. Yamashita, "Analysis of dielectric E-plane waveguides and design of filters," *IEEE Trans. Microwave Theory Tech.*, vol. 46, pp. 1085–1900, Aug. 1988.
[6] A. Abdelmonem *et al.*, "Full-wave design of spurious free D.R. TE mode bandpass filters," *IEEE Trans. Microwave Theory Tech.*, vol. 43, p. 744, Apr. 1995.
[7] S. B. Cohn, "Direct-coupled-resonator filters," *Proc. IRE*, vol. 45, pp. 187–196, 1947.
[8] P. A. Rizzi, *Microwave Engineering Passive Circuits*. Englewood Cliffs, NJ: Prentice-Hall, 1988.
[9] J. S. Izadian and S. M. Izadian, *Microwave Transition Design*. Norwood, MA: Artech House, 1988, pp. 1–8.
[10] J. R. Brews, "Characteristic impedance of microstrip lines," *IEEE Trans. Microwave Theory Tech.*, vol. MTT-35, pp. 30–34, Jan. 1987.
[11] D. Kajfez and P. G. Guillon, *Dielectric Resonators*. Norwood, MA: Artech House, 1986, pp. 467–468.
[12] J. Jin, *The Finite Element Method in Electromagnetics*. New York: Wiley, 1993.
[13] G. Matthaei *et al.*, *Microwave Filters, Impedance-Matching Networks, and Coupling Structures*. Norwood, MA: Artech House, 1980.
[14] H. Y. Hwang, S.-w. Yun, and I.-s. Chang, "A design of bandpass filter using frequency dependent model of inverter immittances," ***<AU: Pls. spell out journal title.>*** *IEEK*, vol. 36-D, pp. 13–20, June 1999.
[15] H. Peng, "Study of whispering gallery modes in double disk sapphire resonators," *IEEE Trans. Microwave Theory Tech.*, vol. 44, pp. 848–854, June 1996.
[16] H. Hwang, N. Park, Y. Cho, S. Yun, and I. Chang, "The design of band-pass filters made of both dielectric and coaxial resonators," in *IEEE MTT-S Int. Microwave Symp. Dig.*, vol. II, 1997, pp. 805–808.
[17] H. Y. Hwang, S. Yun, and I. Chang, "A design of planar elliptic bandpass filter using SMD type partially metallized rectangular dielectric resonators," in *IEEE MTT-S Int. Microwave Symp. Dig.*, vol. III, May 2001, pp. 1483–1486.

Hee Yong Hwang (M'00) was born in Sacheon, Korea, in 1965. He received the B.S. degree in biology and the B.S. degree in electronic engineering from the Seoul National University, Seoul, Korea, in 1988 and 1992, respectively, and the M.S. and the Ph.D. degrees in electronic engineering from Sogang University, Seoul, Korea, in 1995 and 1999, respectively.

From March 2000 to February 2001, he was with the Department of Electronic Engineering, Sogang University, where he was a tenured Professor and with the Amotech Company, as a Research Adviser. He is currently with Department of Electrical and Computer Engineering, University of Maryland at College Park, where he is a Visiting Researcher. His research interests include microwave passive and active filters, and RF systems.

Sang-Won Yun (M'99) was born in Seoul, Korea, in 1954. He received the B.S. and M.S. degrees in electronic engineering from the Seoul National University, Seoul, Korea, in 1977 and 1979, respectively, and the Ph.D. degree in electrical engineering from the University of Texas at Austin, in 1984.

Since September 1984, he has been with the Department of Electronics Engineering, Sogang University, Seoul, Korea, where he is currently a Full Professor. His research interests include microwave and millimeter-wave devices and circuits.

Dr. Yun has served as a Korea T-MTT chapter chairman since January 1999.